Hall-Magnetohydrodynamic Analysis of Acceleration Length and Magnetic Field Optimization in an Argon Hall Thruster

Nadine Barth,[1, a] Kimiya Komurasaki,[2] Dibyesh Satpathy,[3] Jiwon Lee,[1] Maho Matsukura,[4] and Hiroyuki Koizumi[5]

[1] *Graduate Student, Department of Aeronautics and Astronautics, The University of Tokyo*
[2] *Professor, Department of Aeronautics and Astronautics, The University of Tokyo*
[3] *Postdoctoral Researcher, Department of Aeronautics and Astronautics, The University of Tokyo*
[4] *Project Assistant Professor, Department of Aeronautics and Astronautics, The University of Tokyo*
[5] *Professor, Department of Advanced Energy, The University of Tokyo*

(Dated: 24 August 2026)

A zero-dimensional Hall-MHD model is used to examine the influence of magnetic flux density B on the acceleration length L_a and overall performance, using experimental data obtained during argon operation of the RAIJIN66 Hall thruster. The model is derived from the equivalence between electrostatic ion acceleration and electromagnetic thrust generated by the $\mathbf{J} \times \mathbf{B}$ force. The results show that the acceleration length scales approximately as $L_a \propto 1/\sqrt{B}$, consistent with anomalous diffusion theory. Within the investigated range, an increase in acceleration length is associated with improved performance at fixed mass flow rate. A strong dependence on discharge voltage is observed, with operation at 150 V benefiting from reduced magnetic flux density, indicating a MHD-like regime in which an extended acceleration length is advantageous. These findings suggest that the low-voltage regime identified here may be representative of future high-density thruster operation, where reduced magnetic flux density is associated with improved performance.

Keywords: Hall thrusters, alternative propellant, argon, high density, acceleration length, magnetic field

NOMENCLATURE

$A_{r\theta}, A_{zr}$**:** Cross-sectional areas in the axial and azimuthal directions
$\mathbf{B}, B, B_r$**:** Magnetic field (vector, flux density, flux density in radial direction)
e**:** Elementary charge
$\mathbf{E}, E_z$**:** Electric field (vector, axial component)
I_b, I_d, I_e**:** Ion beam, discharge, and electron current
I_H**:** Hall current
I_{sp}**:** Specific impulse
$\mathbf{J}, j_r, j_\theta, j_z$**:** Current density (vector, radial, azimuthal, and axial components)
k**:** Wavenumber
l_θ**:** Azimuthal channel length
L_a, L_i**:** Acceleration length, ionization region length
$\dot{m}_A$**:** Anode mass flow rate
$\dot{m}_i$**:** Ion mass flow rate
m_e, m_i**:** Electron and ion mass
n_e, n_i, n_n**:** Electron, ion, and neutral density
P_D**:** Discharge power
p_e**:** Electron pressure
$r_{\text{in}}, r_{\text{out}}$: Inner and outer channel radii
R_{Plasma}: Plasma resistance
T**:** Thrust
T_e**:** Electron temperature
U_d**:** Discharge voltage
$\mathbf{v}, v_\theta, v_z$**:** Plasma velocity (bulk, azimuthal, axial)
v_{th}, v_i**:** Thermal electron velocity and ion velocity
v_n, v_{nz}**:** Neutral velocity (total, axial)
V**:** Plasma volume
w**:** Channel width
α**:** Anomalous diffusion coefficient
β_e**:** Electron Hall parameter
η_a**:** Anode efficiency
η_u**:** Propellant utilization efficiency
η**:** Plasma resistivity
λ_{De}**:** Electron Debye length
λ_i**:** Ionization mean free path
μ**:** Electron mobility
ν_e, ν_i**:** Effective electron and ion collision frequency
$\nu_{ei}, \nu_{en}, \nu_a$**:** Electron–ion, electron–neutral, and anomalous collision frequency
$\sigma, \sigma_\parallel, \sigma_\perp$**:** Plasma conductivity (total, parallel and perpendicular to B)
σ_{ei}, σ_{en}**:** Electron ion and neutral collision cross section
ω_{ce}**:** Electron cyclotron frequency
ω_{pe}**:** Electron plasma frequency
$\langle \sigma_\mathbf{i} v_\mathbf{e} \rangle$**:** Reaction rate coefficient

[a] Author to whom correspondence should be addressed:n.barth@al.t.u-tokyo.ac.jp

I. INTRODUCTION

Hall thrusters have been used since the early phases of space exploration and are valued for their high specific impulse and long operational lifetime. Xenon is widely regarded as the preferred propellant due to its high atomic mass and relatively low ionization energy. However, its high cost and limited availability have motivated research into alternative propellants. To date, no single alternative has demonstrated comparable overall performance to xenon across operating conditions[1,2]. While alternative propellants, such as argon[3] and krypton[4], show promise, they generally exhibit lower propellant utilization efficiency compared to xenon due to their lower ion mass and reduced ionization rate coefficient[5,6]. To improve the usability of these propellants, alternative approaches that enhance propellant utilization efficiency are required.

Three approaches to improve the propellant utilization efficiency can be identified. The first approach is to extend the ionization length by modifying the magnetic field distribution of the thruster[7–9]. The second is to reduce the axial neutral velocity, thereby increasing the residence time of neutrals in the ionization region. This approach was previously investigated by Satpathy et al. through the introduction of a swirl injector[10] and a sawtooth anode design[11]. These studies reported performance improvements, particularly at low discharge voltages. The third approach is to increase the electron density, which directly enhances the ionization rate. Kim[12] identified this as a key requirement when using alternative propellants.

On one hand, several studies[6,13,14] suggest the existence of a density constraint characterized by a maximum neutral density as a function of discharge voltage, magnetic flux density, and additional operating parameters[13]. Above this value, electron magnetic confinement is weakened due to the increased electron atom collision frequency. The resulting enhancement in electron diffusion causes the electric field to expand spatially, widening the acceleration length while reducing the electric field strength. The characteristic geometry and definition of the acceleration and ionization regions are illustrated in Fig. 1. Consequently, the thruster efficiency decreases due to increased discharge current. Therefore, an increase in neutral density at fixed discharge voltage requires a corresponding increase in magnetic flux density to maintain comparable plasma conditions. On the other hand, Brown and Pinsley[15] reported a linear increase in thrust with propellant flow rate and observed no performance degradation as electron collision frequency increased.

Despite this discrepancy between Dannenmayer[13] and Brown[15], recent studies[16] indicate that Hall thrusters have not yet reached their theoretical thrust density limit. Current devices typically operate at the thrust density of approximately $10\,\mathrm{N/m^2}$, which is well below the theoretical limit of $1000\,\mathrm{N/m^2}$. This limit is primarily constrained by thermal and material considerations. Increasing electron density is essential to approach this limit, as it enhances ionization efficiency and thereby increases thrust. Experimental evidence already indicates that increased neutral density enhances ionization[17–19], and recent high-power-density devices such as H10[20] demonstrate that substantially higher operating densities are technically achievable.

The neutral density can be increased by increasing the mass flow rate $\dot{m}_A$ or by reducing the cross-sectional area $A_{r\theta}$. This increase in neutral density under fixed discharge voltage and magnetic flux density leads to an increase in discharge current density $I_d/A_{r\theta}$. As a result, the discharge power increases, together with the associated thermal load. To maintain comparable plasma impedance and avoid the neutral density limit[13], an increase in magnetic flux density must accompany the increase in mass flow density. In practice, this requires adjustments to the magnetic field configuration, which can influence thruster operational characteristics, including the acceleration length and ionization region length.

Early scaling approaches[21] suggested that magnetic flux density and characteristic length scale are inherently coupled. Kim[12] extended this reasoning by considering acceleration length, indicating that changes in magnetic flux density are expected to influence the effective acceleration region.

However, existing scaling approaches[22–28] do not provide a systematic analysis of the coupled effects of neutral density, magnetic flux density, and acceleration length, particularly for alternative propellants.

In the present study, the neutral density limit defined by Dannenmayer et al.[13] is expected to differ for alternative propellants such as argon because the collision cross sections and ionization characteristics are different. As a result, the density threshold for reduced magnetic confinement may shift, and an increase in neutral density may lead to improved efficiency before confinement effects become dominant.

Therefore, this study investigates the behavior of a Hall thruster under varying neutral and plasma densities, magnetic flux density, and acceleration length in order to identify trends and derive guidance for magnetic field scaling in high-density Hall thruster operation.

At increased electron density, the underlying modeling assumptions must be reconsidered, as enhanced ion–neutral interactions modify ion transport, increase residence time inside the channel, and enhance ionization of neutrals. Under these conditions, the purely electrostatic assumption becomes insufficient, and the plasma behavior approaches that of a magnetized fluid, motivating the use of a Hall-magnetohydrodynamic (Hall-MHD) framework. Based on this approach, a generalized zero-dimensional Hall thruster model is introduced. The model estimates key plasma parameters from experimental data and determines the thrust from the $\mathbf{J} \times \mathbf{B}$ force. The analysis is applied to experimental measurements obtained from the RAIJIN66 thruster[29,30], a Thruster with Anode Layer (TAL) Hall thruster, with particular emphasis on acceleration length estimated from ion beam current measurements.

II. THEORETICAL FRAMEWORK

The theoretical framework presented below is based on a zero-dimensional global model. A cylindrical coordinate system $(r,\ \theta,\ z)$ is used, where z denotes the axial direction along the thruster channel from the anode toward the plume, r is the radial direction, and θ represents the azimuthal direction around the channel. The model assumes that the magnetic flux density B is represented by its peak value and that parameters varying along the z-direction are treated as uniform within the plasma. In addition, standard plasma assumptions such as quasi neutrality, where the electron density n_e equals the ion density n_i ($n_e = n_i$), are applied. This simplified approach allows global trends to be analyzed without introducing additional model complexity. The principal assumptions and limitations of the proposed model are discussed in Section II D.

A. Electron Density Effects on Propellant Utilization Efficiency

As discussed in the introduction, propellant utilization efficiency η_u is a key parameter when evaluating alternative propellants such as argon. It can be expressed using a simplified one dimensional ionization model, as given in Eq. 1:

$$\eta_\mathrm{u} = 1 - \exp\left(-\frac{L_\mathrm{i}}{\lambda_\mathrm{i}}\right) = 1 - \exp\left(-\frac{L_\mathrm{i} n_\mathrm{e} \langle\sigma_\mathrm{i} v_\mathrm{e}\rangle}{v_\mathrm{nz}}\right) \quad (1)$$

Here, L_i denotes the ionization region length, λ_i the ionization mean free path, $\langle\sigma_\mathrm{i} v_\mathrm{e}\rangle$ the ionization rate coefficient, and v_nz the axial neutral velocity, where $v_\mathrm{nz} = 1/4 \cdot v_\mathrm{n}$ and v_n denotes the neutral thermal velocity[10,31].

For alternative propellants such as argon and krypton, the smaller ion mass m_i and ionization rate coefficient $\langle\sigma_\mathrm{i} v_\mathrm{e}\rangle$ result in a lower propellant utilization efficiency compared to xenon, for which η_u is often close to unity under nominal operating conditions.

As introduced in the previous section, one possibility for improving η_u when using alternative propellants is to increase n_e:

$$n_e = \frac{I_b}{e v_i A_{r\theta}} = \frac{\dot{m}_A}{A_{r\theta}} \frac{\eta_u}{v_i m_i}, \quad (2)$$

where I_b denotes the ion beam current, e the elementary charge, v_i the ion velocity, $A_{r\theta}$ the annular cross-sectional area of the discharge channel, and $\dot{m}_A$ the anode mass flow rate.

A recursive effect can further improve η_u, because an increase in the number of ionizing collisions within the channel produces additional electrons. These electrons can subsequently collide again with neutrals, thereby reinforcing the ionization process. This study therefore considers an increase in n_e through increased mass flow density $\dot{m}_A/A_{r\theta}$ as a possible mechanism for improving η_u.

In the present analysis, the mass flow density $\dot{m}_A/A_{r\theta}$ can only be increased within a limited range, as an increase in mass flow rate leads to a rise in discharge current I_d and therefore discharge power P_d exceeding the 2 kW limit of the facility. Therefore, the current analysis focuses on interpreting existing experimental data through the Hall-MHD framework in order to derive scaling guidance for the maximum magnetic flux density and acceleration length.

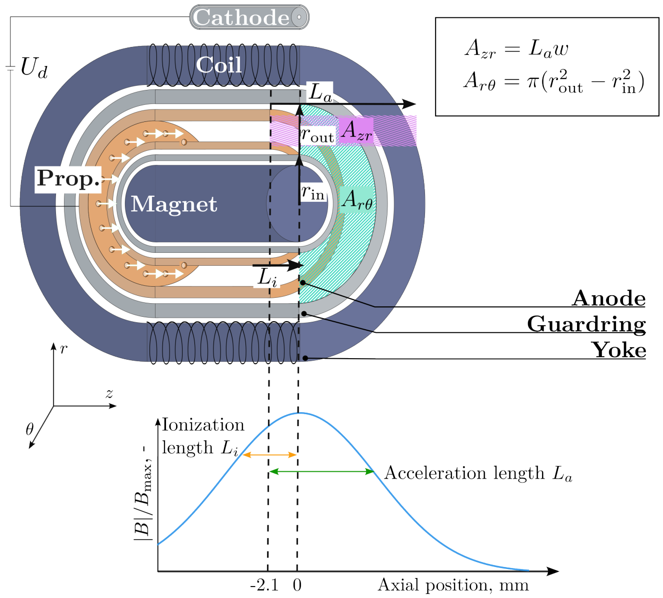

FIG. 1: Schematic of a TAL-type Hall thruster (top) and axial distribution of normalized magnetic flux density (bottom). The characteristic areas $A_{r\theta}$ and A_{zr}, acceleration length L_a, ionization region length L_i, the inner and outer channel radii r_in and r_out, and the channel width w are indicated. The normalized magnetic flux density is given by $|B|/B_\mathrm{max}$.

The ionization region length is defined inside the hollow anode as the region extending from approximately 80% of the maximum B to the guard-ring exit, resulting in a total length of 5.6 mm for RAIJIN66[7]. The acceleration length L_a is assumed to begin at the anode exit and to overlap with L_i until the guard-ring exit (see Fig. 1). Its magnitude is estimated from experimental operating conditions.

Recent particle-in-cell (PIC) studies have demonstrated that both the peak position and axial gradient of the magnetic flux density influence electron transport and overall thruster performance[9,32,33]. In the present work, however, the magnetic field topology is kept fixed. The zero dimensional analysis used in this study considers only the maximum magnetic flux density and does not include two dimensional effects such as magnetic field gradients. Therefore, only the magnitude of the peak magnetic flux density is varied, while the spatial distribution is flat and gradient is neglected.

B. Hall-MHD Formulation Relating Thrust, Hall Current, and Acceleration Length

As stated in the introduction, this work adopts a Hall-MHD interpretation of Hall thruster operation. In the conventional electrostatic description, ions are accelerated by the axial electric field E and exhausted from the channel without significant interaction with neutrals. Ions are treated as unmagnetized, and ion–neutral collisions are neglected.

At increased plasma density, ion–neutral collisions increase the ion residence time and modify momentum transport. Under these conditions, the plasma is more appropriately described as a conducting fluid, providing the motivation for adopting a Hall-MHD framework.

Following the formulation of Huba[34], Hall-MHD is described by the conservation of mass and momentum together with the generalized Ohm's law. The present work does not solve the complete Hall-MHD system. Instead, the momentum equation provides the basis for interpreting thrust as the volume-integrated Lorentz force, while the generalized Ohm's law is used to determine the current density distribution required for the zero-dimensional model. Consequently, only the Hall-MHD relations required for the present analytical formulation are retained.

Accordingly, the generalized Ohm's law is expressed as

$$\mathbf{E} + \mathbf{v} \times \mathbf{B} - \frac{\mathbf{J} \times \mathbf{B}}{n_e e} + \frac{\nabla p_e}{n_e e} - \eta \mathbf{J} = \frac{1}{\omega_{pe}^2} \frac{d\mathbf{J}}{dt}, \quad (3)$$

where $\mathbf{E}$ denotes the electric field vector, $\mathbf{v}$ the plasma velocity vector, $\mathbf{B}$ the magnetic flux density vector, $\mathbf{J}$ the current density vector, p_e the electron pressure, η the plasma resistivity, and ω_{pe} the electron plasma frequency. The terms represent the ideal MHD contribution, Hall effect, electron pressure gradient, resistive (Ohmic) diffusion, and electron inertia, respectively.

The electron inertia term is neglected in the present model. Its validity was assessed by comparison with the Lorentz force in the electron momentum equation. Using a representative magnetic flux density of the RAIJIN66 Hall thruster ($B = 45\,\mathrm{mT}$) together with a characteristic electron momentum relaxation time, the electron inertia is estimated to be approximately 6% of the Lorentz force. Since this estimate depends on the ratio of the electron momentum relaxation time to the electron cyclotron period, it remains valid for both classical and anomalous electron diffusion, provided that electron magnetization is maintained.

The electron pressure gradient was assessed by comparison with the Lorentz force density. Using representative operating conditions of the RAIJIN66 Hall thruster ($n_e = 1 \times 10^{17}\,\mathrm{m^{-3}}$, $T_e = 20\,\mathrm{eV}$, and $L = 10\,\mathrm{mm}$) gives an electron pressure gradient of approximately $32\,\mathrm{N\,m^{-3}}$. Assuming a uniform force distribution over the acceleration volume ($L = 10\,\mathrm{mm}$, $A_{zr} = 6.72 \times 10^{-5}\,\mathrm{m^2}$), the Lorentz force density estimated from the measured thrust is approximately $4.5 \times 10^4\,\mathrm{N\,m^{-3}}$. The Lorentz force therefore dominates the momentum balance under the representative operating conditions considered for the RAIJIN66 Hall thruster, supporting the simplified Hall-MHD formulation adopted in this work.

These assumptions are therefore valid for the operating conditions considered here. When the electron inertia or electron pressure gradient becomes comparable to the Hall or resistive terms, the complete generalized Ohm's law should be retained. Under the present conditions, Eq. (3) reduces to

$$\mathbf{E} + \mathbf{v} \times \mathbf{B} = \eta \mathbf{J} + \frac{1}{e n_e} (\mathbf{J} \times \mathbf{B}). \quad (4)$$

For further simplicity, the electric field $\mathbf{E}$ is assumed to have only an axial (z) component, while the magnetic field $\mathbf{B}$ is assumed to be purely radial (r). To estimate the current densities, the electron velocity in the axial direction v_z is neglected. In addition, the electron azimuthal velocity is approximated by the $\mathbf{E} \times \mathbf{B}$ drift velocity, $v_\theta = E_z/B_r$[35], leading to

$$j_\theta = \sigma v_z B_r - \mu B j_z \approx -\mu B_r j_z = -\beta_e j_z \quad (5)$$

$$j_z = \frac{\sigma_\parallel E_z}{1 + \beta_e^2} = \sigma_\perp E_z \quad (6)$$

where σ denotes the electrical conductivity and μ the electron mobility. Within the Hall-MHD framework, the Hall current density j_θ and its coupling to the axial current density j_z are explicitly described by the electron Hall parameter β_e.

$$\beta_e = \frac{j_\theta}{j_z}. \quad (7)$$

This formulation enables the analysis of electromagnetic forces, in particular the $\mathbf{J} \times \mathbf{B}$ force, and establishes the electron Hall parameter as a link between thrust T and the discharge current I_d.

In classical kinetic Hall thruster theory, thrust is calculated as the reaction force resulting from electrostatic ion acceleration using the ion mass flow rate $\dot{m}_i$ and the ion velocity v_i,

$$T_{\text{electrostatic}} = \dot{m}_i v_i. \quad (8)$$

In the present work, however, the Hall-MHD formulation is adopted, in which thrust is interpreted as the net electromagnetic body force acting on the plasma. Under steady operating conditions, integrating the axial component of the Lorentz force over the plasma volume yields the total electromagnetic thrust,

$$T_{\text{MHD}} = \int (\mathbf{J} \times \mathbf{B})_z \, dV = \int j_\theta B_r \, dV = I_H B l_\theta, \quad (9)$$

where dV denotes the differential plasma volume, I_H is the Hall current, and l_θ is the mean azimuthal length of the channel. Although derived from different physical perspectives, Eqs. (8) and (9) describe the same measurable thrust.

As introduced in Eq. 7, the electron Hall parameter relates the current densities in the z- and θ-directions. In the following, β_e is used to relate the Hall current density to the experimentally measured thrust and currents. The electron Hall parameter can also be written as

$$\beta_e = \frac{j_\theta}{j_z} = \frac{I_H/A_{zr}}{I_e/A_{r\theta}}, \tag{10}$$

where I_H and I_e denote the Hall current and the electron current, respectively. The areas represent the cross sections through which the respective currents flow. The axial current density passes through the thruster cross sectional area $A_{r\theta}$, while the azimuthal current density is associated with the area A_{zr}.

The effective length associated with A_{zr} is not uniquely defined, because the azimuthal current does not flow through a geometrically fixed cross section. In the present analysis, A_{zr} is approximated using L_a and the effective channel width w.

In the next step, the electron current is determined. It is approximated as the difference between discharge current I_d and ion beam current I_b,

$$I_e = I_d - I_b. \tag{11}$$

I_b corresponds to the portion of the discharge current transported by ions that are accelerated through the channel and contribute directly to thrust generation. It is measured experimentally using an ion collector plate[7].

Using the assumptions introduced above, the electron Hall parameter can be expressed as a function of the thrust, magnetic flux density, discharge current, ion beam current, and acceleration length:

$$\begin{aligned}\beta_e &= \frac{I_H}{I_e}\frac{A_{r\theta}}{A_{zr}} \\ &= \frac{T}{B\,(I_d - I_b)}\frac{\pi(r_{out}^2 - r_{in}^2)}{L_a w l_\theta}.\end{aligned} \tag{12}$$

This relation establishes a link between electron current and thrust. In contrast to the electrostatic approach, where thrust is obtained from the ion acceleration, the Hall-MHD formulation relates both quantities through the electromagnetic body force acting on the plasma. As a result, the thrust can be expressed in terms of discharge quantities such as I_e, without isolating individual ion acceleration processes.

By rearranging Eq. 12, L_a can be determined from the experimentally obtained I_b, B, and I_d. Equation 13 therefore provides a direct means of estimating the acceleration length from measurable discharge quantities and should be regarded as an estimation equation rather than a theoretical scaling law.

$$L_a = \frac{T}{B\,(I_d - I_b)\,\beta_e}\frac{\pi(r_{out}^2 - r_{in}^2)}{w l_\theta}. \tag{13}$$

The present Hall-MHD framework does not explicitly resolve ionization processes. Instead, ionization effects are implicitly contained in the experimentally measured quantities, but are not modeled as a separate physical process.

C. Electron Diffusion in the Acceleration Region

In a Hall thruster, cross field electron transport plays a central role in determining efficiency and overall performance. Under ideal conditions, electrons are magnetized and follow classical diffusion behavior driven by collisions with neutrals or ions. However, experimental observations show that electron transport exceeds classical predictions. This deviation is referred to as anomalous diffusion and is commonly attributed to plasma turbulence, fluctuations, or instabilities, particularly in regions with strong electric and magnetic field gradients[36]. In the following, an anomalous diffusion regime is assumed.

In classical diffusion, the total electron collision frequency is given by the sum of the electron-ion and electron-neutral collision frequencies:

$$\nu_e = \nu_{ei} + \nu_{en} = n_i\langle\sigma_{ei}v_{ei}\rangle + n_n\langle\sigma_{en}v_{en}\rangle, \tag{14}$$

where n_i and n_n denote the ion and neutral densities, respectively, and $\langle\cdot\rangle$ represents averaging over the electron velocity distribution function. The cross sections are obtained from LXCAT[37] and averaged over the velocity distribution using Bolsig+[38].

In the anomalous diffusion regime, the effective electron collision frequency includes an additional anomalous term ν_a, which represents an effective scattering rate accounting for turbulence. The total electron collision frequency is therefore written as:

$$\nu_e = \nu_{ei} + \nu_{en} + \nu_a, \tag{15}$$

where $\nu_a = \alpha\omega_c = \alpha eB/m_e$ and α is an empirical coefficient describing the strength of anomalous transport. Bohm diffusion represents an empirical upper bound for cross field electron transport in magnetized plasmas and is commonly used as a reference model for anomalous transport in Hall thrusters.

The electron Hall parameter, introduced in Eq. 7, characterizes the degree of electron magnetization and directly influences cross field transport. It can also be expressed as

$$\beta_e = \frac{\omega_{ce}}{\nu_e} = \frac{eB}{m_e\nu_e}, \tag{16}$$

where ω_{ce} is the electron cyclotron frequency. Under classical diffusion conditions, β_e typically reaches values of several hundred, whereas experimental observations often indicate smaller values. The experimentally determined electron Hall parameters obtained using Eq. 7 therefore corresponds to smaller values associated with anomalous diffusion.

A common modeling assumption[35] is Bohm diffusion with $\alpha = 1/16$, which yields $\nu_e = eB/(16m_e)$ and results in $\beta_e = 16$. Reported values may vary depending on thruster configuration and operating conditions. For xenon operation, PIC simulations are available[39,40]. These studies indicate that for the UT58 thruster[41–43], operating with xenon, the effective electron mobility in the acceleration region is well approximated by a Bohm mobility corresponding to $\beta_e = 32$. Both the UT58 and the RAIJIN-66 are high-power TAL-type Hall thrusters with comparable outer channel diameters and xenon mass flow rates. Therefore, this value is adopted as a representative approximation for xenon operation in the present 0D scaling model. In particular, because magnetically shielded SPT-type Hall thrusters primarily accelerate the plasma outside the thruster, the same physical interpretation is expected to be applicable to such configurations. Therefore, this value is adopted here as a representative approximation for xenon operation in the present 0D scaling model. Therefore, in the following analysis $\beta_e = 16$ is adopted for argon, while $\beta_e = 32$ is used for xenon.

D. Model Limitations

The proposed model is a zero-dimensional scaling model intended to identify global trends rather than to predict the detailed plasma structure within the discharge channel. Consequently, the acceleration lengths obtained from the present analysis should be interpreted as representative scaling parameters that capture the relative influence of magnetic flux density, discharge voltage, and mass flow rate, rather than as the actual physical acceleration lengths.

The model further assumes that the magnetic flux density is represented by its peak value and that plasma properties varying along the axial direction are replaced by representative values. Likewise, the anomalous electron transport is represented by a fixed Hall parameter. In reality, the effective electron mobility depends on the local magnetic flux density, plasma properties, thruster geometry, and operating conditions, resulting in an axial variation of the Hall parameter and anomalous transport coefficient. Accordingly, the analytical derivation presented here is valid only while these assumptions remain satisfied; otherwise, the derived scaling relations are not expected to remain applicable without accounting for the additional physical effects.

Although the present validation is performed using a TAL-type Hall thruster, the proposed scaling methodology is derived from the fundamental $E \times B$ acceleration mechanism rather than from geometry-specific features. In particular, magnetically shielded SPT-type Hall thrusters are physically similar to TAL thrusters because, in both cases, the plasma is primarily accelerated outside the discharge channel. Therefore, the underlying physical interpretation is expected to be qualitatively applicable to magnetically shielded SPT-type Hall thrusters as well. Nevertheless, quantitative differences arising from wall interactions and magnetic field distributions may affect the exact scaling coefficients.

III. DESIGN AND OPERATIONAL PARAMETERS OF THE TAL THRUSTER RAIJIN66

This section presents the thruster configurations, the experimental operating conditions, and the measured performance results of RAIJIN66.

A. RAIJIN66 Anode Configurations

The thruster analyzed in this study is RAIJIN66, which was scaled down from RAIJIN94 by Hamada[29,30]. In its original configuration, the copper anode consists of an indented and protruding profile toward the channel exit[7].

The original design was intended for axial propellant injection. It was subsequently modified by Satpathy et al.[10] to introduce directional propellant injection, referred to in this work as swirl flow.

In addition, a straight anode configuration without the original geometry was developed to enable comparison with the proposed sawtooth anode design, which incorporates a reduced anode exit area[44].

The three anode configurations considered in this study are shown in Fig. 2 (a) to (c).

B. RAIJIN66 magnetic field design

B is a key parameter in the Hall-MHD analysis and is therefore discussed in detail. The magnetic field configuration of RAIJIN66 is shown in Fig. 2 (d). The peak magnetic flux density, which corresponds to $z = 0$, is located at the channel exit, while the anode tip shown in Fig. 2 is located at $z = -2.1$ mm. The configurations considered here correspond to the RAIJIN66 version without a trim yoke and thus without magnetic shielding[7].

In the global model, the maximum magnetic flux density near the thruster exit is used. The corresponding peak magnetic flux densities are 30 mT (dotted green), 45 mT (dashed orange), and 60 mT (solid blue). The magnetic flux density distribution was computed using FEMM, and the peak value at the channel exit was validated experimentally with a magnetic field probe (Model MG-801, Kanetec Co., Ltd.).

C. Experimental Setup

All experiments were conducted at the University of Tokyo. A detailed description of the experimental setup is provided by Satpathy[10,44–47].

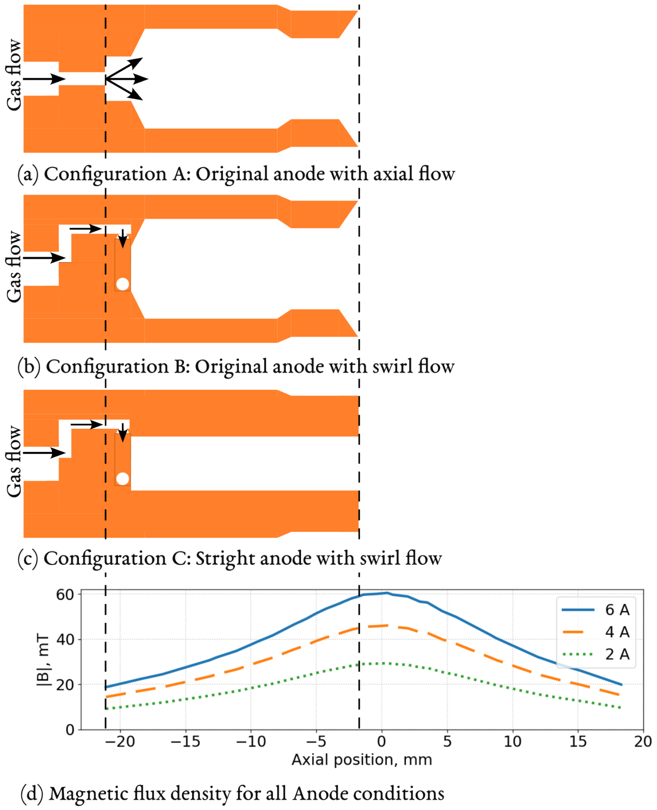

FIG. 2: (a) to (c): RAIJIN66 anode configurations: the original anode with axial flow (a), the original anode with swirl flow (b), and the straight anode with swirl flow (c). (d) Axial magnetic flux density distribution for different coil currents.

The experimental data used in this analysis were obtained over a wide range of anode temperatures[46]. In the present analysis, the data are averaged over the duration of each experiment to obtain representative operating values, thereby reducing the influence of startup transients and differences in experiment duration. As the objective of the present study is to investigate overall trends rather than exact quantitative values, this averaging procedure is not expected to affect the qualitative conclusions of this work. The analyzed datasets correspond to anode temperatures between approximately 350 K and 400 K. Assuming that the neutral gas temperature follows the anode temperature while all other plasma parameters remain unchanged, this temperature variation is estimated to introduce a variation of approximately 5.3% in the ion beam current. Accordingly, the data, even under similar operating conditions, are influenced by temperature induced effects, and the discussion therefore focuses on overall trends rather than absolute values.

The acceleration length is estimated based on experimental thrust data. Thrust measurements were performed using a double pendulum thrust stand[10], and ion beam measurements were obtained using an ion collector plate[7]. The acceleration length is estimated using the reference thrust measurement together with the ion beam current measurements. The reference thrust was measured using a double-pendulum thrust stand[10], while the ion beam current was measured using an ion collector plate[7]. In this analysis, ion beam current measurements are used to estimate η_u as

$$\eta_u = \frac{I_b m_i}{e \dot{m}_A}. \quad (17)$$

Measured thrust data were available only at selected operating points. To extend the dataset, thrust was estimated using a scaling relation consistent with electrostatic acceleration[35], expressed as a function of I_b and discharge voltage U_d:

$$\frac{T}{T_0} = \frac{I_b}{I_{b,0}} \sqrt{\frac{U_d}{U_{d,0}}}. \quad (18)$$

Here, the subscript 0 denotes the reference operating point ($U_d = 150\,\mathrm{V}$, $I_d = 5\,\mathrm{A}$, $B = 30\,\mathrm{mT}$, corresponding to approximately 750 W), for which the thrust was measured using the dual-pendulum thrust stand. The remaining thrust values were estimated using Eq. (18), which is intended to capture the overall trend across the investigated operating conditions rather than provide exact quantitative predictions. Comparison with the available direct thrust measurements indicates that the scaling slightly underestimates the thrust at higher discharge powers while preserving the overall trend.

The complete dataset shown in Fig. 3 comprises 86 experiments conducted with RAIJIN66, including 79 experiments with argon as the propellant and 7 with xenon. The xenon data serve as a validation reference and were obtained with the straight anode configuration (Configuration C) under a single magnetic flux density setting for comparison with the argon data. In addition, the 300 V operating condition was investigated at a single magnetic flux density setting. The experimental operating conditions considered in this study are summarized in Table I.

TABLE I: Summary of the operating conditions investigated in the present study. Some of the experimental data included in this study were previously reported by Satpathy et al.[10,44–47], which also provide details of the corresponding experimental procedures.

Parameter	Values
Discharge voltage U_d	150 V, 200 V, 250 V, 300 V†
Mass flow rate (argon) $\dot{m}_A$	2.0 mg/s, 2.8 mg/s
Mass flow rate (xenon) $\dot{m}_A$	2.7 mg/s
Magnetic flux density B	30 mT, 45 mT, 60 mT

† $B = 30, 45\,\mathrm{mT}$ for $U_d = 150, 200\,\mathrm{V}$; $B = 45\,\mathrm{mT}$ for 300 V only.

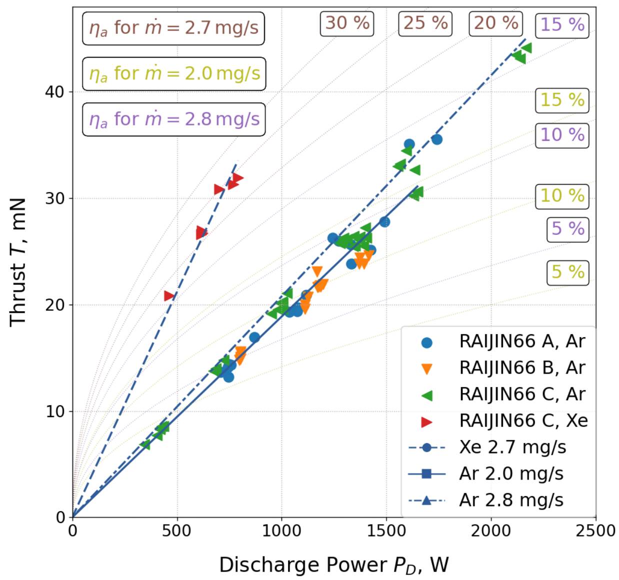

FIG. 3: Thrust T as a function of discharge power P_D for the RAIJIN66 thruster under all investigated operating conditions. Symbols denote the different anode configurations, while line styles represent the propellant mass flow rates. Dotted lines indicate fixed anode efficiency η_a.

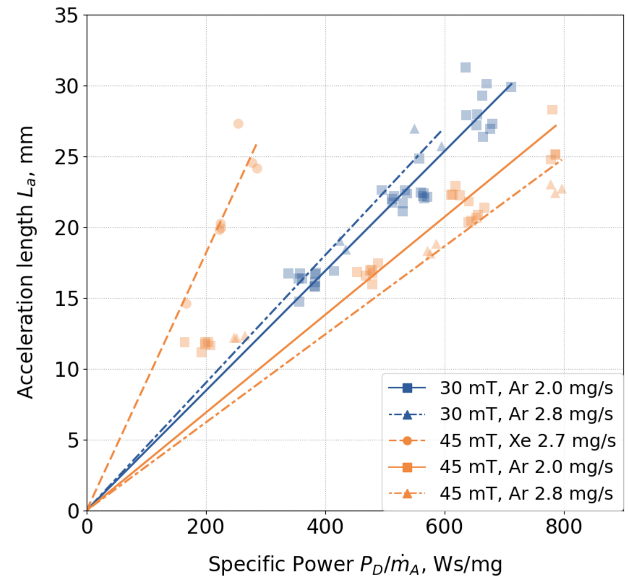

FIG. 4: Acceleration length L_a as a function of specific power $P_D/\dot{m}_A$. Colors distinguish the magnetic flux densities, while line styles and symbols indicate the corresponding linear fits for the different mass flow rates.

D. Performance of RAIJIN66

Figure 3 shows the thrust as a function of discharge power P_D, used to estimate L_a for all experiments considered in this study. The dashed lines indicate the anode efficiency, where brown, yellow, and purple correspond to 2.7 mg/s xenon, 2.0 mg/s argon, and 2.8 mg/s argon, respectively. The solid lines represent fixed mass flow rates and show that the thrust increases approximately linearly with discharge power over the investigated range for a given mass flow rate. Throughout this study, the error bars indicate the spread of the experimental data within each operating condition and are intended to illustrate the variability of the dataset rather than the measurement uncertainty.

For higher mass flow rates, and thus higher neutral densities, slightly higher thrust values are observed at comparable discharge power. For the higher argon mass flow rate condition, labeled as 2.8 mg/s, two slightly different experimental values were used: 2.7 mg/s at 45 mT and 2.9 mg/s at 30 mT. These two operation conditions are combined in the following analysis to enable comparison across different magnetic flux densities.

The xenon data shows lower thrust values compared to the nominal design performance of RAIJIN66. This is because the xenon mass flow rate was chosen to match the argon mass flow rate for comparison. The thruster was originally designed to operate at 3.3 mg/s. However, operation at this mass flow rate with argon was not possible within the available facility power limits.

Figure 3 further shows that, despite the use of three different anode configurations, the overall thrust trends remain comparable across all cases when evaluated at similar discharge power. This indicates similar behavior among the investigated configurations and justifies their combined analysis.

IV. RESULTS

A. Acceleration Region Length Estimated from Electrostatic and Electromagnetic Acceleration Equivalency

Using the equations introduced in Section II, L_a is estimated from Eq. 13 by assuming that the thrust derived from the magnetohydrodynamic $\mathbf{J} \times \mathbf{B}$ force is equivalent to the electrostatic thrust given in Eq. 18.

Figure 4 presents the resulting acceleration lengths. The linear fits are constrained to pass through the origin to emphasize the proportionality between acceleration length and specific power. This constraint is motivated by the expected scaling behavior, although the low specific power regime is not experimentally accessible in the present study. The constrained fit is therefore intended only to illustrate the proportional relationship over the investigated operating range and is not intended as an extrapolation toward zero specific power. At sufficiently low specific power, the assumptions of the analytical model may no longer be valid, and additional physical mechanisms may become important.

Figure 4 shows that the estimated acceleration length

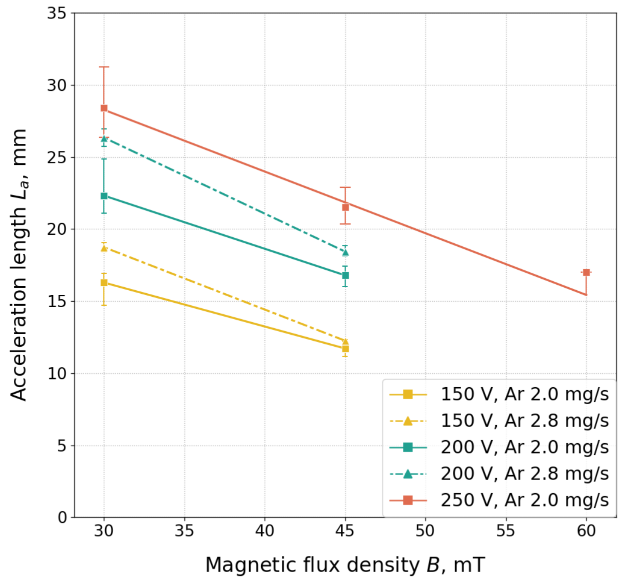

FIG. 5: Acceleration length L_a as a function of magnetic flux density B. Colors distinguish the discharge voltages, while symbols and line styles distinguish the mass flow rates. Error bars represent the spread of the experimental data.

increases approximately linearly with the specific discharge power for all investigated operating conditions. Differences between the datasets are primarily associated with magnetic flux density and propellant type.

At low specific power(approximately 150–300 Ws/mg in Fig. 4), the data correspond to reduced discharge voltage conditions (150 V) and show a systematic deviation from the linear fit constrained through the origin. The underlying cause of this deviation is discussed in detail in Section V C.

It can also be observed that a higher B leads to a shorter L_a under fixed mass flow rate conditions, consistent with the expected scaling and is discussed in more detail in the following subsection.

B. Dependency of the Acceleration Length on Magnetic Flux Density

To further investigate the influence of magnetic confinement, the estimated acceleration length is plotted as a function of magnetic flux density.

Figure 5 shows that the acceleration length decreases with increasing magnetic flux density for all investigated operating conditions. In addition, higher discharge voltages and mass flow rates are generally associated with larger acceleration lengths at a given magnetic flux density. Despite these differences, all datasets exhibit a similar overall dependence on magnetic flux density.

To quantify this dependence, the experimental data were fitted using a power-law relationship. The resulting average slope is approximately -0.5, corresponding to

$$L_a \propto \sqrt{\frac{1}{B}}. \tag{19}$$

C. Performance Improvement with Increasing Acceleration Length

The electric field scales with U_d and L_a (Eq. 20), so increasing L_a at fixed U_d reduces the electric field strength. Within the Hall-MHD framework, this primarily affects electron transport and the overall plasma dynamics.

In addition to this effect, changes in the electric field may also influence ionization processes, which are not explicitly captured by the present model. In particular, a reduced electric field may lead to a decrease in ionization efficiency, potentially increasing losses[48]. These ionization-related effects are therefore considered as an additional mechanism superposed on the MHD behavior, especially at higher discharge voltages.

It has been shown in simulations[49] that shifting the magnetic flux density maximum outside the channel is associated with a shallower potential drop and therefore a larger L_a. The performance initially improves, but beyond a ratio $B_{\text{exit}}/B_{\max} = 0.9$, where B_{exit} denotes the magnetic flux density at the channel exit, a strong decrease in efficiency is observed due to the reduced electric field strength.

However, most of these studies focus on xenon as the propellant. Due to the high propellant utilization efficiency typically achieved with xenon, an extended plasma region is often unnecessary and may increase collision related losses. In contrast, for alternative propellants with lower ionization efficiency, the extension of the acceleration region can be beneficial[50].

For RAIJIN66, where neither xenon nor argon reach propellant utilization efficiencies close to unity under the investigated conditions, an increase in L_a may improve thruster performance. The dependence of I_{sp} and η_a on L_a is therefore evaluated.

Figure 6(a) shows the dependence of I_{sp} on L_a. A nonlinear trend is observed, with I_{sp} increasing over the investigated range and approaching saturation as L_a increases. A similar trend is observed for η_a, as shown in Figure 6(b).

The data indicate that, at fixed mass flow rate, an increase in L_a is associated with improved thruster performance within the investigated range. The nonlinear behavior suggests that thrust and efficiency approach a plateau as L_a increases, indicating that beyond a certain point further increases in L_a do not yield additional performance gains.

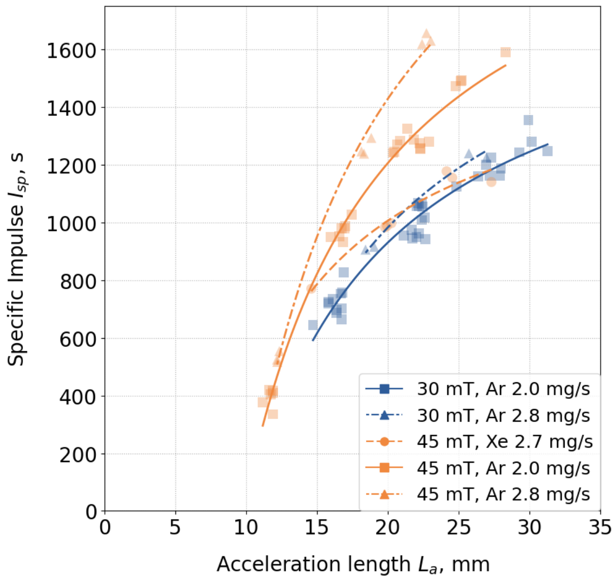

(a) Specific impulse I_{sp}

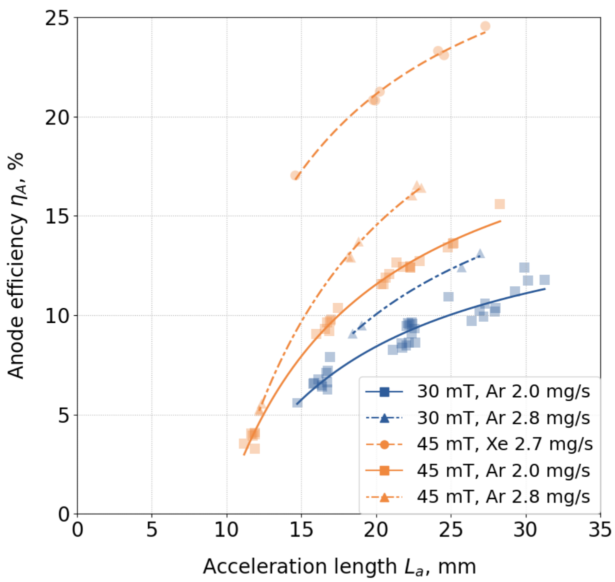

(b) Anode efficiency η_a

FIG. 6: Specific impulse I_{sp} and anode efficiency η_a as functions of acceleration length L_a. Colors distinguish the magnetic flux densities, while line styles and symbols indicate the corresponding linear fits for the different mass flow rates.

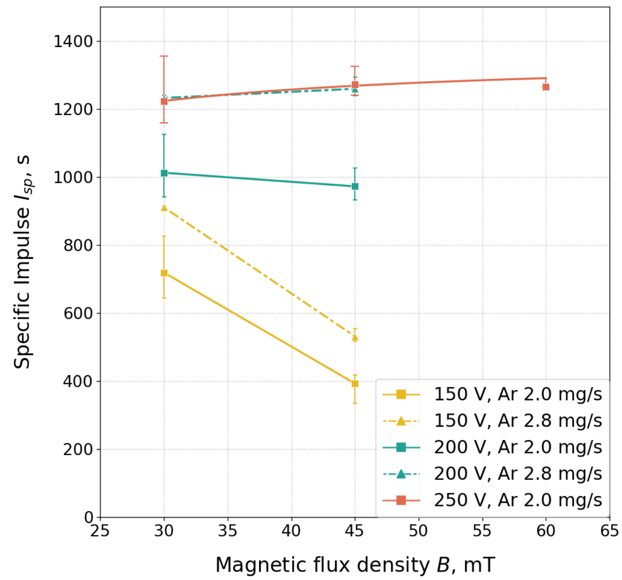

(a) Specific impulse I_{sp}

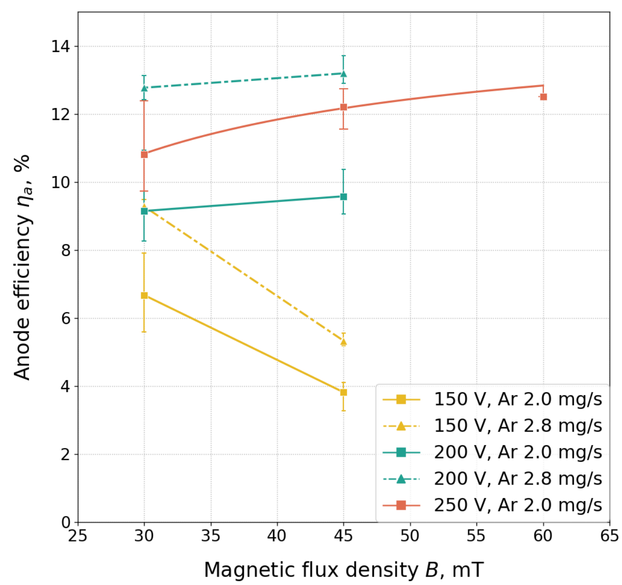

(b) Anode efficiency η_a

FIG. 7: Specific impulse I_{sp} and anode efficiency η_a as functions of magnetic flux density B. Colors distinguish the discharge voltages, while symbols and line styles distinguish the mass flow rates. Error bars represent the spread of the experimental data.

D. Dependency of Performance on Magnetic Flux Density at Fixed Mass Flow Rate

The previous analysis showed that an increase in L_a can improve thruster performance. According to Eq. 19, a decrease in B corresponds to an increase in L_a. The following subsection examines whether this implied benefit of reduced B is observed in the experimental data.

Figure 7(a) shows the expected increase of I_{sp} with decreasing B at fixed discharge voltage of 150 V for both investigated mass flow rate conditions. However, at increased discharge voltages, this dependence becomes weak and remains approximately unchanged within the experimental uncertainty. This weak dependence on B at increased discharge voltages may be related to increased ionization efficiency at elevated electron temperatures.

Figure 7(b) shows the corresponding η_a. A similar trend is observed, with improved performance at low discharge voltages for decreasing magnetic flux densities, while at higher voltages the trend reverses and higher magnetic flux densities become favorable.

At 150 V, the optimal magnetic flux density for maximizing η_a appears to lie below the lowest tested B of 30 mT. At 200 V, the optimum is expected between 45 mT and 60 mT based on Fig. 7. At 250 V, the optimal magnetic flux density appears to lie above the investigated range.

These observations demonstrate that the optimal magnetic flux density shifts systematically toward higher values with increasing discharge voltage, indicating that the magnetic field scaling changes with the operating voltage.

V. DISCUSSION

The presented results indicate that an Hall-MHD-based interpretation of thrust provides additional insight into the coupling between magnetic confinement, acceleration length, and discharge power. In particular, the observed trends suggest a strong interaction between magnetic flux density and acceleration length that influences thruster performance. The following discussion examines the underlying physical mechanisms and their implications for high-density Hall thruster operation.

A. Influence of Anomalous Diffusion on Acceleration Length and Plasma Resistance

The experimental results presented in Section IV B indicate an approximate dependence of $L_a \propto 1/\sqrt{B}$. This differs from the $L_a \propto 1/B$ dependence commonly assumed in previous studies[12,21,48]. The following discussion examines whether anomalous electron diffusion provides a physical explanation for this difference.

A classical estimate of the acceleration length is given by

$$E = \frac{U_d}{L_a}. \tag{20}$$

This expression shows that, in addition to the dependence on B, U_d must also be considered when analyzing L_a.

According to Erofeev and Zharinov[51] and Kim[12], the acceleration length length may be approximated by

$$L_a \approx \sqrt{\frac{m_e U_d}{eB^2}\frac{\nu_e}{\nu_i}}, \tag{21}$$

where ν_i is the ionization frequency. This relation was later supported experimentally by Khayms[21] and Chhavi et al.[48].

The experimentally observed $1/\sqrt{B}$ dependence suggests that the assumption of classical electron transport may not be sufficient to describe the present operating

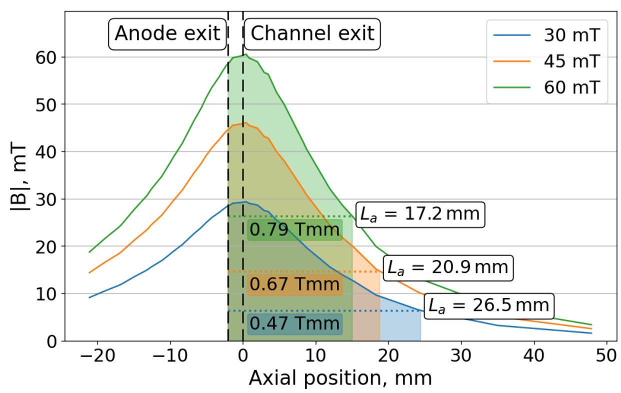

FIG. 8: Acceleration length L_a represented geometrically within the magnetic flux density distribution of the thruster for 1200 W at fixed $\dot{m}_A = 2.0$ mg/s. Shaded areas indicate $\int B\,dz$, with the values shown corresponding to the respective integrals.

conditions. Therefore, an alternative description based on anomalous electron diffusion is considered.

Instead of adopting classical diffusion as Kim[12], the present analysis considers anomalous diffusion with an effective electron collision frequency proportional to B as presented in section II C. Combining these relations with the previously introduced dependence of the electric field on L_a leads to the following scaling for the acceleration length:

$$L_a \approx \sqrt{\frac{\alpha U_d}{\nu_i B}}. \tag{22}$$

This scaling is consistent with the observed data and indicates that anomalous diffusion provides a plausible explanation for the deviation from the classical 1/B dependence reported in the literature. Because this scaling is derived under the assumption that anomalous electron diffusion dominates the electron mobility, its applicability is linked to the validity of this transport mechanism under the investigated operating conditions.

To further interpret the observed dependence on magnetic flux density, the spatial distribution of the acceleration length relative to B is considered. Figure 8 shows the axial magnetic flux density distribution together with the geometrical representation of L_a for different magnetic flux densities. For fixed mass flow rate and discharge power conditions, a decrease in magnetic flux density leads to an extension of the acceleration length.

According to anomalous diffusion theory, the plasma resistance R_{Plasma} depends on the magnetic flux density and the acceleration length:

$$\begin{aligned} R_{\text{Plasma}} &= \eta \frac{L_a}{A_{r\theta}} \\ &= \frac{B}{e n_e \alpha}\frac{L_a}{A_{r\theta}} \propto \frac{B L_a}{\alpha n_e}. \end{aligned} \tag{23}$$

This expression assumes a spatially uniform magnetic flux density. However, as shown in Fig. 8, the magnetic flux density varies along the axial direction. A more appropriate formulation with respect to the magnetic-field distribution is therefore obtained by integrating the local resistivity over the acceleration region:

$$R_{\text{Plasma}} \propto \frac{\int_0^{L_a} B\, dz}{\alpha n_e}. \tag{24}$$

In the present zero-dimensional model, however, the electron density is represented by a characteristic value over the acceleration region rather than by its local axial distribution. Consequently, Eq. (24) represents a simplified expression for the effective plasma resistance. A more rigorous evaluation would require the local electron-density profile and evaluation of $\int B(z)/n_e(z), dz$. Nevertheless, the present formulation remains suitable for examining the relative influence of the magnetic-field distribution.

Therefore, the integral $\int_0^{L_a} B\, dz$ is shown in Fig. 8, representing the magnetic flux density integrated over the acceleration region. It can be observed that this integral increases with increasing magnetic flux density and therefore also increases the effective plasma resistance predicted by Eq. (24).

To examine whether this relationship is reflected experimentally, the plasma resistance is shown in Fig. 9. An overall increase in plasma resistance with increasing magnetic flux density can be observed across all operating conditions.

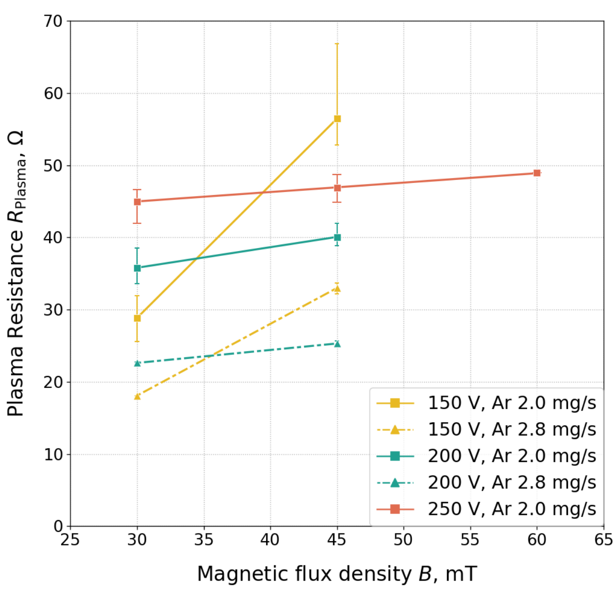

FIG. 9: Plasma resistance R_{Plasma} as a function of magnetic flux density B. Colors distinguish the discharge voltages, while symbols and line styles distinguish the mass flow rates. Error bars represent the spread of the experimental data.

This trend is consistent with the increase of $\int_0^{L_a} B\, dz$ shown in Fig. 8, suggesting that, within the present simplified model, higher magnetic flux densities are associated with increased effective plasma resistance and consequently higher resistive losses.

These results indicate that anomalous diffusion affects not only the scaling of the acceleration length but also the resistive properties of the plasma. Reduced magnetic flux densities therefore result in an extended acceleration region and reduced plasma resistance, which can contribute to improved thruster performance for certain operating regimes.

B. Influence of the Acceleration length and Magnetic Flux Density onto Thruster Performance

Section IV C showed that, for a fixed mass flow rate, both I_{sp} and η_A increase with increasing acceleration length. This contrasts with common assumptions in the literature, where an extended acceleration length is associated with a reduced electric field strength and reduced electron confinement, leading to enhanced axial electron transport and modified collision dynamics within the channel. In addition, a reduced magnetic flux density is typically associated with a reduced plasma potential due to the increased acceleration length.

Experimental results by Chhavi et al.[48] support this view, showing that under fixed discharge power conditions a decrease in magnetic flux density leads to reduced thrust and ion beam current. In that study, the magnetic flux density distribution was modified while maintaining fixed discharge power through adjustments of the propellant mass flow rate.

In contrast, the present analysis does not impose fixed discharge power. Instead, the discharge current adjusts to the imposed mass flow rate and magnetic flux density, resulting in variations in discharge power even at fixed discharge voltage. Consequently, a reduction in B is not necessarily accompanied by a decrease in available discharge power, which explains the deviation from the trends reported by Chhavi et al.[48]. With variable discharge current and discharge power, a decrease in B does not necessarily lead to reduced thruster performance.

The observed discrepancy indicates that a more detailed constraint on the magnetic flux density and acceleration length is required. In the literature, the permissible range of the acceleration length is often constrained by the electron and ion Larmor radii:

$$\frac{m_e v_e}{eB} \ll L_a \ll \frac{m_i v_i}{eB}. \tag{25}$$

These criteria are typically satisfied over a wide range of magnetic flux densities. More restrictive guidelines were proposed by Ding et al.[8], who observed different scaling behavior depending on the discharge voltage. At lower voltages, the relation $B \propto \sqrt{U_d}$ was found, whereas at increased voltages above 450 V the dependence changed to $B \propto U_d$, which was attributed to the saturation of the electron temperature T_e. Variations in electron temperature due to changes in plasma density, as reported by Fossum[52], are neglected both in that study and in the present analysis, as density variations during Hall thruster operation are assumed to be small. In addition, the optimal operating conditions identified in their study correspond to nearly steady discharge current.

A similar trend was reported by Shirasu et al.[53], who observed no increase in propellant utilization efficiency above 250 V when using water vapor, which was attributed to electron temperature saturation. These findings suggest that the propellant species may influence the voltage at which this transition occurs.

In contrast to these observations, the present experimental results in Section IV D show that, at a discharge voltage of $U_d = 150\,\mathrm{V}$, higher anode efficiency occurs at reduced magnetic flux density and is associated with higher discharge current. This trend suggests that the governing processes at $U_d = 150\,\mathrm{V}$ differ from those observed under higher voltage conditions. This difference can be attributed to the lower ion velocity at reduced discharge voltage, because the ion acceleration is directly governed by the discharge potential. The reduced ion velocity increases the ion residence time within the acceleration region, making collisional interactions more important and reducing the validity of a purely electrostatic description. Consequently, these conditions are more consistent with a fluid-based Hall-MHD interpretation.

Based on these observations, a transition for the RAIJIN66 thruster between low-voltage (150 V) and high-voltage (250–300 V) operation is suggested. It is expected that the latter is influenced by the increased ionization efficiency at higher electron temperatures.

Hall thrusters are often operated at discharge voltages above 300 V, as increased voltages result in larger ion velocities and therefore higher I_{sp}. At these voltages, reduced discharge current is typically associated with higher anode efficiency. In contrast, the present study shows that, at a discharge voltage of $U_d = 150\,\mathrm{V}$, higher I_{sp} and η_a can be achieved at reduced magnetic flux densities and high discharge current.

Future high-density thrusters are expected to exhibit increased collisional interactions, which modify ion transport and increase residence time within the channel. The increased collision frequency reduces the validity of treating ions as collisionless particles that are directly accelerated by the electrostatic potential. Instead, collective plasma behavior becomes increasingly important, making a fluid-based Hall-MHD description more appropriate.

In this regime, the low discharge voltage conditions considered in the present analysis appear to be more representative and are therefore relevant for future high density thruster designs. In contrast, high voltage operation is dominated by electrostatic acceleration with higher acceleration efficiency and lies outside the Hall-MHD framework considered here, and is therefore less representative for such designs.

Additional design approaches, such as swirl flow[10] and sawtooth anode geometries[11], have demonstrated improved efficiency at lower discharge voltages. Combining these approaches with reduced magnetic flux density may provide further performance improvements and inform future Hall thruster design.

C. Recommendation for High Density Hall Thruster Design

The Hall-MHD analysis presented in this study provides insight into the relationship between acceleration length, magnetic flux density, and mass flow rate. Based on these results, recommendations for the maximum magnetic flux density design of future high density Hall thrusters are derived.

In the previous section, it was shown that the optimal magnetic flux density for the RAIJIN66 thruster depends strongly on the discharge voltage. A voltage-dependent transition in the magnetic field scaling has also been reported by Ding et al.[8], although at a higher discharge voltage. This suggests that the transition between the low- and high-voltage operating regimes depends on the thruster geometry and operating conditions, including the plasma density, rather than occurring at a universal discharge voltage. Consequently, no universal voltage-dependent scaling criterion is proposed in the present work. Instead, the following recommendations for future high-density Hall thrusters are discussed separately for low- and high-discharge-voltage operating regimes. The transition voltage between these regimes is expected to depend on the thruster geometry and operating conditions and therefore needs to be determined individually for each thruster.

At low discharge voltage (150 V for RAIJIN66), the optimal magnetic flux density appears to lie below the lowest tested value of 30 mT, based on an extrapolation of the experimental data (Fig. 7). However, such low magnetic flux densities lead to increased discharge currents. Under these operating conditions, the primary limitation arises from the associated increase in power demand and thermal load, which are constrained by the available power generation and thermal management capabilities of the spacecraft. The magnetic flux density must therefore also be considered as a parameter for power and thermal management in practical thruster design. This regime is referred to as an MHD-like regime, as the reduced ion velocity requires a magnetohydrodynamic interpretation of the plasma behavior.

At increased discharge voltages (250–300 V for RAIJIN66), the available data suggest that the optimal magnetic flux density lies above 60 mT, which is not accessible with the present thruster design. This trend is consistent with observations reported in the literature and is referred to here as the electrostatic regime. Although a precise recommendation cannot be given for these voltages, the results indicate that the optimal magnetic flux density increases with discharge voltage.

Between these regimes, an intermediate transition regime is observed at 200 V for RAIJIN66, where the optimal magnetic flux density stagnates at approximately 45–60 mT. This condition is the only case where an increase in the estimated electron density (Eq. 2) leads to a reduction in anode efficiency, indicating a change in the dominant performance mechanisms.

At low discharge voltages, reduced magnetic flux density results in higher estimated electron density together with improved propellant utilization efficiency and anode efficiency. At increased discharge voltages, improved current utilization due to higher ionization rates leads to a larger ion beam current and therefore improved performance, where increased η_u is associated with increased electron density. This indicates that, in the transition regime represented by the 200 V condition, increasing the electron density does not lead to improved performance and should therefore be avoided in high density thruster operation.

Future high density thrusters are expected to operate at increased electron densities, leading to enhanced ion–neutral collisions. These collisions increase ion residence time, resulting in operating conditions where an MHD-like interpretation becomes more appropriate, similar to the low voltage regime identified in this study. It remains unclear whether the transition regime shifts with increasing electron density. However, it is expected that the corresponding transition voltage increases, as reduced ion velocities may extend the range over which MHD-like behavior is observed.

For the design of high density thrusters, scaling relations that deviate from classical approaches may therefore be required. In particular, reduced magnetic flux densities may be advantageous under high density conditions. Consequently, the magnetic circuit should be designed to provide a wide adjustable range of magnetic flux densities in order to accommodate different operating regimes and to manage thermal loads.

VI. CONCLUSION

This study investigates the use of argon as an alternative propellant to xenon for Hall thrusters. A zero dimensional Hall-MHD framework was developed based on the equivalence between electrostatic and electromagnetic thrust.

Using experimental data from the RAIJIN66 TAL Hall thruster, the model reveals that the acceleration length follows an approximate $L_a \propto 1/\sqrt{B}$ scaling. This behavior differs from the classical $1/B$ dependence commonly reported in the literature and is consistent with anomalous diffusion theory.

Furthermore, the results indicate that an increase in L_a at fixed mass flow rate can improve thrust and anode efficiency. As L_a depends on B, it is generally expected that a reduced B can increase performance. This influence of magnetic flux density on performance depends on the discharge voltage, with improved performance observed at 150 V, whereas no improvement is observed at > 250 V due to higher ionization rates.

Operation around 150 V defines a regime in which a Hall-MHD interpretation becomes useful, as reduced ion velocities increase ion residence time and collisional interactions. The physical mechanisms in this regime differ from those typically reported in Hall thruster literature and are expected to become increasingly relevant for high-density thrusters, where enhanced plasma density increases ion–neutral collisions, modifies ion transport, and increases residence time within the channel.

Based on these observations, recommendations for magnetic flux density design as a function of discharge voltage are derived. In the low-voltage regime, a reduction in magnetic flux density improves performance, with the main limitation being the increased thermal load on the thruster.

An intermediate voltage regime is identified in which increasing the electron density n_e does not lead to improved efficiency, whereas a high-voltage regime shows typical electrostatic behavior with increasing efficiency for increased n_e. For high-density thrusters, this regime is expected to shift to higher voltages than those tested in this study.

These findings indicate that the optimal magnetic flux density does not correspond to the lowest discharge current condition. Instead, reduced magnetic flux density combined with a larger effective acceleration length may improve overall thruster performance under high-density operation conditions.

ACKNOWLEDGMENTS

This work was supported by KAKENHI Grant Numbers 24KJ0766 and 25K01416 from the Japan Society for the Promotion of Science.

AUTHOR DECLARATIONS

Conflict of Interest

The authors have no conflicts to disclose.

Author Contributions

N. Barth: Conceptualization (supporting); Methodology (lead); Formal analysis (lead); Investigation (supporting); Data curation (lead); Validation (equal); Visualization (lead); Writing – original draft (lead). **K. Komurasaki**: Conceptualization (lead); Validation (equal); Resources (equal); Supervision (lead); Writing – review & editing (equal). **D. Satpathy**: Investigation (lead); Validation (equal); Writing – review & editing (equal).

J. Lee: Validation (equal); Writing – review & editing (equal). **M. Matsukura**: Validation (equal); Writing – review & editing (equal). **H. Koizumi**: Resources (equal).

DATA AVAILABILITY

The data that support the findings of this study are available from the corresponding author upon reasonable request.

REFERENCES

[1] V.-G. Tirila, A. Demairé, and C. N. Ryan, Acta Astronautica **212**, 284 (2023).
[2] J. J. Szabo, M. Robin, S. Paintal, B. Pote, and V. Hruby, in *48th AIAA/ASME/SAE/ASEE Joint Propulsion Conference and Exhibit* (2012) AIAA-2012-3853.
[3] J. Yamasaki, S. Yokota, and K. Shimamura, Vacuum **167**, 520 (2019).
[4] J. A. Linnell and A. D. Gallimore, Journal of Propulsion and Power **22**, 1402 (2006).
[5] P. Nagy, A. Skutlartz, and V. Schmidt, Journal of Physics B: Atomic and Molecular Physics **13**, 1249 (1980).
[6] T. Munro-O'Brien and C. Ryan, Acta Astronautica **206**, 257 (2023).
[7] D. Satpathy, H. Sekine, N. Barth, R. Kawashima, K. Komurasaki, and H. Koizumi, Transactions of the Japan Society for Aeronautical and Space Sciences **68**, 12 (2025).
[8] Y. J. Ding, L. Q. Wei, D. C. Jia, and D. R. Yu, Physica Scripta **89**, 085602 (2014).
[9] H. Fan, H. Li, Y. Ding, L. Wei, and D. Yu, Advances in Space Research **66**, 2024 (2020).
[10] D. Satpathy, H. Sekine, J. Lee, K. Komurasaki, R. Kawashima, and H. Koizumi, Journal of Applied Physics **136**, 233301 (2024).
[11] D. Satpathy, K. Komurasaki, J. Lee, H. Sekine, N. Barth, and H. Koizumi, Journal of Applied Physics **139**, 083303 (2026).
[12] V. Kim, Journal of propulsion and power **14**, 736 (1998).
[13] K. Dannenmayer and S. Mazouffre, in *31st International Electric Propulsion Conference* (Ann Arbor, MI, USA, 2009) IEPC-2009-077.
[14] K. Dannenmayer and S. Mazouffre, Journal of Propulsion and Power **27**, 236 (2011).
[15] C. O. Brown and E. A. Pinsley, AIAA Journal **3**, 853 (1965).
[16] J. Simmonds, Y. Raitses, and A. Smolyakov, Journal of Electric Propulsion **2**, 12 (2023).
[17] I. Kronhaus and A. Linossier, Plasma Sources Science and Technology **27**, 124005 (2018).
[18] O. Hamo and I. Kronhaus, Journal of Applied Physics **130**, 223303 (2021).
[19] I. Kronhaus and A. Linossier, in *39th International Electric Propulsion Conference* (2024) IEPC-2024-425.
[20] R. R. Hofer, J. B. Simmonds, D. M. Goebel, J. M. Steinkraus, and A. R. Payman, Journal of Electric Propulsion **4**, 35 (2025).
[21] V. Khayms and M. Martinez-Sanchez, in *32nd Joint Propulsion Conference and Exhibit* (Lake Buena Vista, FL, USA, 1996) AIAA-1996-3291.
[22] M. Andrenucci, L. Biagioni, S. Marcuccio, and F. Paganucci, in *28th International Electric Propulsion Conference* (2003) p. 1721.
[23] T. Misuri, F. Battista, C. Barbieri, E. A. De Marco, M. Andrenucci, *et al.*, in *30th International Electric Propulsion Conference* (2007) IEPC-2007-311.
[24] T. Misuri and M. Andrenucci, in *44th AIAA/ASME/SAE/ASEE Joint Propulsion Conference & Exhibit* (2008) p. 4806.
[25] A. A. Shagayda and O. A. Gorshkov, Journal of Propulsion and Power **29**, 466 (2013).
[26] A. A. Shagayda, IEEE Transactions on Plasma Science **43**, 12 (2014).
[27] Y. V. Plyashkov, A. A. Shagayda, D. A. Kravchenko, A. S. Lovtsov, and F. D. Ratnikov, Journal of Propulsion and Power **38**, 935 (2022).
[28] T. Lafleur and P. Chabert, Plasma Sources Science and Technology **34**, 055005 (2025).
[29] Y. Hamada, R. Kawashima, K. Komurasaki, N. Yamamoto, H. Tahara, and T. Miyasaka, in *35th International Electric Propulsion Conference* (2017) IEPC-2017-412.
[30] Y. Hamada, R. Kawashima, J. Bak, K. Komurasaki, and H. Koizumi, Vacuum **186**, 110040 (2021).
[31] B. M. Reid, *The influence of neutral flow rate in the operation of Hall thrusters* (University of Michigan, 2009).
[32] Q. Liu, Y. Li, Y. Hu, and W. Mao, Aerospace **10**, 942 (2023).
[33] C. Chhavi and M. L. Walker, Plasma Sources Science and Technology **34**, 115006 (2025).
[34] J. D. Huba, in *Space Plasma Simulation*, edited by J. Büchner, C. T. Dum, and M. Scholer (Springer, Berlin, Heidelberg, 2003) pp. 166–192.
[35] D. M. Goebel, I. Katz, and I. G. Mikellides, *Fundamentals of electric propulsion* (John Wiley & Sons, 2023).
[36] F. F. Chen, *Introduction to plasma physics and controlled fusion* (Springer, 2016).
[37] L. C. Pitchford, L. L. Alves, K. Bartschat, S. F. Biagi, M.-C. Bordage, I. Bray, C. E. Brion, M. J. Brunger, L. Campbell, A. Chachereau, *et al.*, Plasma Processes and Polymers **14**, 1600098 (2017).
[38] G. Hagelaar and L. C. Pitchford, Plasma sources science and technology **14**, 722 (2005).
[39] J. Bak, R. Kawashima, J. Simmonds, and K. Komurasaki, Physics of Plasmas **28**, 102510 (2021).
[40] J. Bak, R. Kawashima, G. Romanelli, and K. Komurasaki, Journal of Applied Physics **131**, 053302 (2022).
[41] T. Schönherr, R. Kawashima, H. Koizumi, and K. Komurasaki, in *33rd International Electric Propulsion Conference* (2013) IEPC-2013-242.
[42] D. Fujita and K. Komurasaki, Vacuum **110**, 159 (2014).
[43] J. Bak, Y. Hamada, Y. Hirano, K. Komurasaki, T. Schönherr, and H. Koizumi, in *52nd AIAA/SAE/ASEE Joint Propulsion Conference* (2016) p. 4625.
[44] D. Satpathy, H. Sekine, J. Lee, N. Barth, and K. Komurasaki, in *39th International Electric Propulsion Conference* (2025) IEPC-2025-106.
[45] D. Satpathy, *Control of Neutral Gas Dynamics for High Efficiency Argon Hall Thrusters*, Ph.D. thesis, The University of Tokyo, Tokyo, Japan (2025).
[46] D. Satpathy, S. Kawabata, H. Sekine, R. Kawashima, K. Komurasaki, and H. Koizumi, Journal of Electric Propulsion **2**, 5 (2023).
[47] D. Satpathy, H. Sekine, J. Lee, N. Barth, and K. Komurasaki, in *39th International Electric Propulsion Conference* (2025) IEPC-2025-107.
[48] C. Chhavi and M. L. Walker, Journal of Electric Propulsion **5**, 3 (2026).
[49] D. Yongjie, P. Wuji, W. Liqiu, S. Guoshun, L. Hong, and Y. Daren, Journal of Physics D: Applied Physics **49**, 465001 (2016).
[50] F. Marchioni and M. A. Cappelli, Journal of Applied Physics **130** (2021).
[51] V. S. Erofeev and A. V. Zharinov, in *Plasma Accelerators* (Mashinostroenie, Moscow, Russia, 1972) pp. 65–67.
[52] E. Fossum and L. King, in *44th AIAA/ASME/SAE/ASEE Joint Propulsion Conference and Exhibit* (2008) AIAA-2008-5190.
[53] K. Shirasu, K. Ikeda, N. Hirota, H. Koizumi, H. Sekine, and K. Komurasaki, Transactions of the Japan Society for Aeronau-

tical and Space Sciences **69**, 51 (2026).